Electrochemically Driven Hydroxyapatite Nanoparticles Coating of Medical Implants

Ori Geuli, Noah Metoki, Noam Eliaz, and Daniel Mandler**

Calcium phosphates are of great interest for biomedical applications such as bone tissue engineering, bone fillers, drug and gene delivery, and orthopedic and dental implant coating. Here, the first electrochemically driven coating of medical implants using hydroxyapatite (HAp) nanoparticles (NPs) as building blocks is reported. This uncommon combination offers a simple, straightforward, and economic process with well controllable, pure, single-phase HAp. Crystalline, pure HAp NPs are formed by precipitation reaction. The HAp NPs are dispersed by either citrate or poly(acrylic acid) to form pH sensitive dispersion. Controllable and homogeneous coating of medical implants is accomplished by altering the pH on the surface upon applying either a constant potential or current. The process involves protonation of the carboxylic acid moieties, which causes the irreversible aggregation of the HAp NPs due to diminishing the repulsive forces between the particles. Deposition is further demonstrated on a commercial dental implant. Moreover, the adhesion of the coating satisfies FDA and international standard requirements. A porous interconnected network of bone-like HAp layer is formed during soaking in a simulated body fluid for 30 d and is similar to bone generation, and it therefore holds promise for further in vivo testing.

1. Introduction

Orthopedic and dental implants are vastly used nowadays in reconstructive medicine.[1] Alloys, mainly titanium-based, are used to fabricate these implants.[2] Coatings are often applied to improve the osteoconductivity and osseointegration.[3–5] By far, coating of titanium with calcium phosphate (CaP) ceramics has become the dominant approach in this field. CaPs represent a family of materials consisted of various phases, among others, hydroxyapatite (HAp), α- and β-tricalcium phosphate, and octacalcium phosphate.[6] The CaP coating increases both the bioactivity and biocompatibility of the implant, forming direct bonds with the adjacent tissue, thus enhancing osseointegration and promoting bone regeneration.[7] HAp, $Ca_5(PO_4)_3(OH)$, has been studied extensively for a variety of applications, such as bone cements, bone fillers, bone tissue engineering, drug and gene delivery, etc.[8] This is due to its chemical and structural similarity to biological apatite, which is the prime inorganic constituent of bone.[9]

Currently, HAp coatings can be formed by several processes, such as plasma spraying, laser pulse deposition, sol–gel coating, electrophoretic and electrochemical deposition.[10] Some of these techniques are expensive, form nonuniform coatings, and do not allow very precise control of the process. For example, plasma spraying, the most common method in industry today, is a non-line-of-sight technique which forms a variety of poorly crystalline phases on the implant's surface and introduces residual thermal stresses that eventually result in delamination and failure.[10,11] Another example is electrophoretic deposition (EPD) of HAp.[1,3] This process involves applying high voltage to the substrate, and therefore the HAp nanoparticles (NPs) must be calcined before deposition in order to evaporate adsorbed water.[12] Furthermore, EPD requires densification by sintering the coating at high temperatures.[13] Electrochemical deposition is a low-cost, simple, and flexible technique for coating conductive substrates.[3,6,10] Electrochemical deposition of HAp from aqueous solutions is associated with local altering of pH in the vicinity of the cathode surface as a result of water reduction, which causes the precipitation of CaP from solution.[13–15]

Electrodeposition of HAp can be carried out in two different manners, depending on the building blocks used in the process—ions or NPs. Starting with ionic species, i.e., calcium and phosphate ions, might form some undesired CaP phases in the coating. Hence, there is significant advantage in using NPs as the building blocks, thus dictating in advance the chemical composition and phase content of the resulting deposit. Moreover, nanoparticulate HAp possesses significant benefits, such as enhanced densification, improved fracture toughness and elevated osteoconductivity due to its high surface area.[16] Higher osteoconductivity by HAp NPs is attributed to the increased adsorption, adhesion, differentiation, and proliferation of osteoblasts.[17,18] In addition, HAp NPs enhance the deposition of

O. Geuli, Prof. D. Mandler
Institute of Chemistry
the Hebrew University of Jerusalem
Jerusalem 9190401, Israel
E-mail: daniel.mandler@mail.huji.ac.il
N. Metoki, Prof. N. Eliaz
Biomaterials and Corrosion Lab
Department of Materials Science and Engineering
Tel-Aviv University
Ramat Aviv 6997801, Israel
E-mail: neliaz@tau.ac.il

DOI: 10.1002/adfm.201603575

bone minerals on its surface, and therefore increase the development of a new bone tissue shortly after implantation.[18] It is known that HAp NPs can be synthesized by various approaches, including precipitation reaction, hydrothermal synthesis, sol-gel process, biomimetic deposition, flame spray pyrolysis process,[19] and microemulsion synthesis.[17,20]

Thus, combining electrochemical deposition and HAp NPs seems to offer both the advantages of a simple and straightforward technique with the formation of a controllable coating made of a HAp phase per se. Very few studies by which HAp NPs can be electrochemically deposited have been reported. For example, Thiemig et al. electrochemically deposited HAp-ZnFe nanocomposite film.[21] Pang and Zhitomirsky reported on EPD of HAp promoted by chitosan electrodeposition to create HAp-chitosan nanocomposite on stainless steel substrate in mixed water–ethanol solution.[22] Park and Jang reported on electrodeposition of HAp NPs onto TiO_2 nanotube layer under high potential (28 V) in an electrolyte containing NH_4F and $(NH_4)H_2PO_4$.[7]

Here, we present a novel approach for electrochemical deposition of pure HAp NPs, which have been formed by precipitation reaction under mild potentials, for coating titanium substrates (**Scheme 1**). The electrodeposition was successfully performed, using well-defined HAp NPs dispersed in aqueous solution using water soluble stabilizing agents—tri-sodium citrate (Cit) and sodium polyacrylate (PAA). Deposition produces high purity, single phase, HAp coating under both potentiostatic and galvanostatic conditions. The process is driven by applying positive potential (<3 V), which oxidizes water causing a reduction in the pH in vicinity of the implant surface. This results in the protonation of the carboxylic residues of the dispersants and diminishes the repulsion interactions among the NPs, thus driving irreversible aggregation of the particles.

2. Results and Discussion

2.1. Preparation and Characterization of HAp NPs

HAp NPs were synthesized via precipitation reaction from a solution of calcium nitrate into which diammonium phosphate solution was dropwise added (as described in Scheme 1). Figure 1S (Supporting Information) shows SEM images of the HAp NPs in aqueous solution. It can be seen that the NPs are elongated. Dynamic light scattering gave an average size of ≈94 ± 40 nm. The NPs are similar to those reported previously[10,23,24] using this precipitation method. Furthermore, energy-dispersive X-ray spectroscopy (EDS) and X-ray photoelectron spectroscopy (XPS) analysis of the powder (Table 1S, Supporting Information) was performed. In addition, EDS spectrum and element mapping of the powder is provided in Figure 2S (Supporting Information). EDS showed that the ratio of Ca/P is 1.56 ± 0.04. This value is somewhat close to that of stoichiometric HAp (1.67). It should be noted that EDS analysis is not recommended for unambiguous distinction between different CaP phases.[25] In XPS measurement carbon

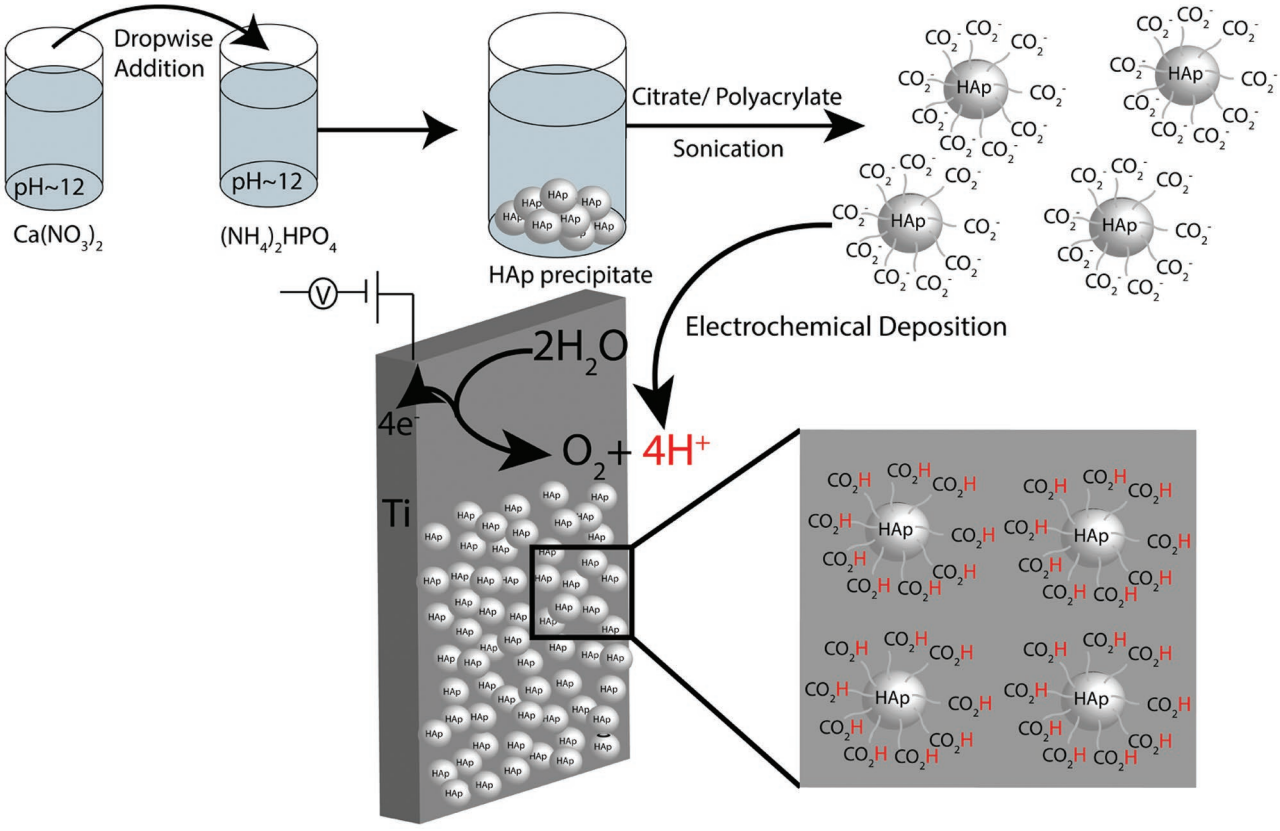

Scheme 1. Schematics of the electrochemical deposition of HAp NPs on Ti.

is present in the spectra, which is related to CO_2 contamination. The results indicate a similar Ca/P ratio of 1.58, which is yet somewhat lower than that of stoichiometric HAp. To further clarify the phase content, X-ray diffraction (XRD) measurements were conducted. Figure 3S (Supporting Information) shows the XRD pattern of the HAp NPs. All reflections were assigned to the HAp phase (ICSD-PDF2 file 01-084-1998).[26] No other CaP phases were detected. The degree of crystallinity of the HAp NPs calculated from the XRD is ≈70%.[27]

We note that all previous studies involved the electrochemical deposition of HAp from ionic-molecular species.[7,14] The concept of this work is to start with well-defined HAp NPs dispersed in solution and cause their controlled deposition. In our case, stabilizing the HAp NPs is achieved by carboxylic acids, which enable their electrochemical deposition by induced protonation of the acid. The approach is based on applying a positive potential in aqueous solutions, which causes the formation of protons upon oxidation of water and, thus, the decrease of the pH on the electrode surface.[28] Hence, we examined the ζ-potential and size of the NPs as a function of pH to assure that a decrease of pH causes their aggregation and precipitation. It should be noticed that our method differs substantially from EPD as the latter requires high voltage and is based on the migration of particles under electrical field.[7,12,13,23,29]

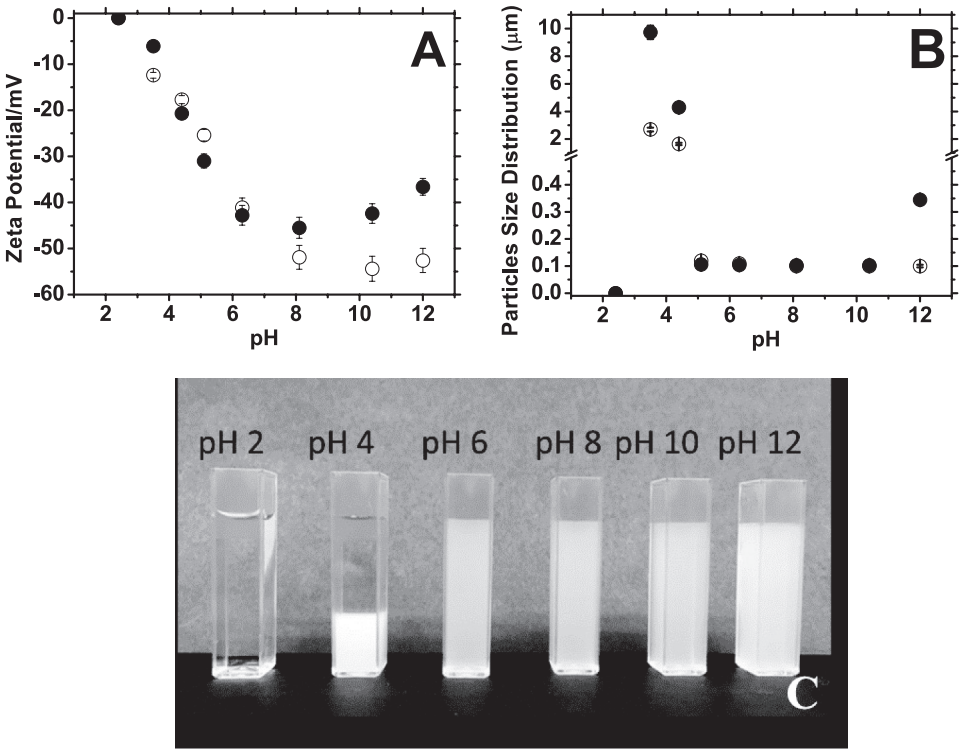

Figure 1. A) ζ-potential, and B) particle size distribution of HAp NPs dispersed by Cit (red) and PAA (black) as a function of pH. C) Image of Cit-stabilized HAp nanoparticle suspensions as a function of pH. The pH was changed by adding HCl (0.5 M) or NaOH (0.5 M).

HAp NPs were stabilized by two acids; Cit and PAA, the pK_A of which is 3.13, 4.76, 6.39, and 4.25,[30] respectively. This implies that the HAp NP dispersions are expected to be stabilized due to the strong negative repulsion between the NPs at pH > pK_A, and at the same time will be destabilized at pH < pK_A. The change in the dispersion stability can be studied by measuring the ζ-potential and particle size distribution as a function of pH (**Figure 1**).

It is evident that the decrease of pH affects the stability of both dispersions, i.e., stabilized by Cit and PAA. The ζ-potential shows a sigmoidal behavior where the particles attain negative potential of ≈–50 mV at pH > 8, while at pH < 3 the total charge of the NPs diminishes. The inflection point is at ≈pH 4, which is in good agreement with the pK_{A2} of Cit and pK_{A1} of PAA. Furthermore, the change of the ζ-potential with pH matches the change in particle size. The sharp decrease of the particles' size at pH < 3 is due to their dissolution. This is also supported by the images of the dispersions (Figure 1C). A stable dispersion is obtained as pH > 5, whereas lowering the pH yields initially an opaque solution (due to increasing the NPs size). All these results indicate that by altering the pH, namely, decreasing it below pH < 4–5, we destabilize the HAp dispersion and cause their precipitation.

2.2. Electrochemical Deposition and Coating Characterization

The next step comprised the electrochemical deposition of the stabilized HAp NPs dispersion onto Ti surfaces. We conducted a series of tests studying the effect of various applied potentials (1.5–2.5 V Ag/AgCl [1 M]) and duration on the deposition (not shown here). The application of a positive potential drives the oxidation of water on the anode and generation of protons

$$2H_2O \rightarrow O_2 + 4H^+ + 4e^- \quad (1)$$

Figure 2A,B shows a typical SEM image of the Cit-stabilized HAp NPs on Ti deposited at 2 V for 25 min. It can be seen that the deposition is uniform and resembles the shape of the initial NPs (Figure 1S, Supporting Information). It is conceivable that electrochemical deposition is also particularly suitable for template deposition using micrometer scale structures such as polystyrene particles.[31] This template deposition may allow the selective deposition on implant's surface as well as the creation of microporous films. Varying the deposition potential had no effect on the nature of the deposit. Yet, it can be seen that the thickness of HAp coating increases as the applied potential is raised up to ≈2 V, where it levels off (Figure 2C). Therefore, we decided to apply a potential of 2 V for the following

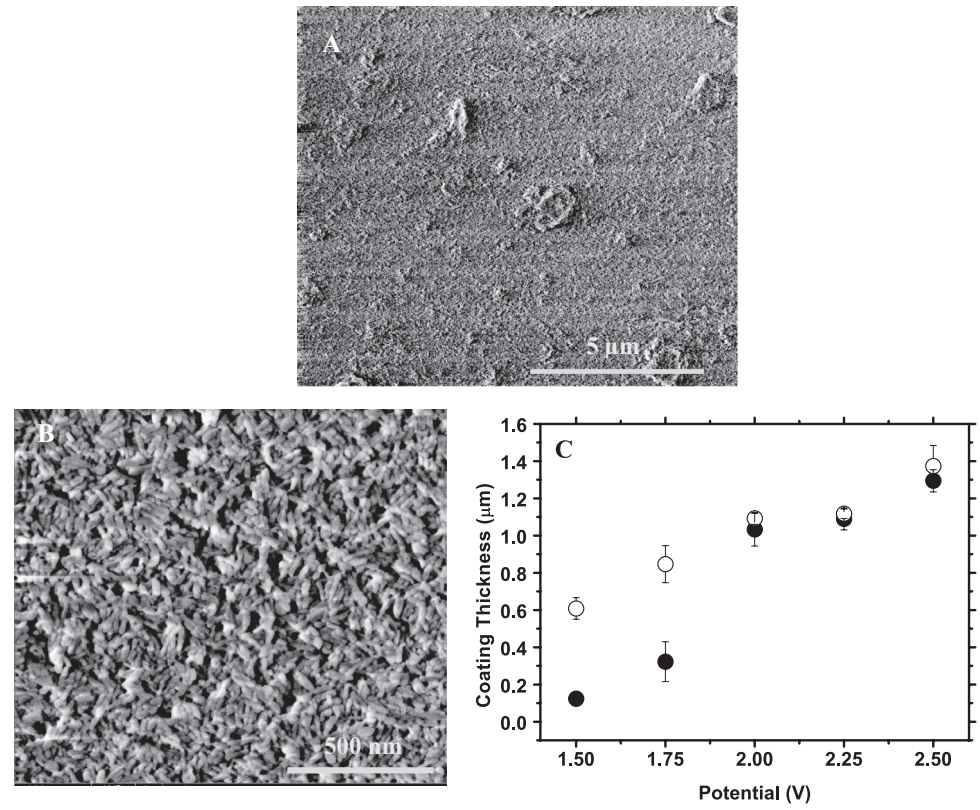

Figure 2. A,B) XHR-SEM image of HAp NPs stabilized with Cit (10×10^{-3} M) and electrochemically deposited at 2 V for 25 min. C) Thickness of the HAp NPs coating as a function of the applied potential for both dispersions ($t = 25$ min). Black dots: PAA-stabilized HAp NPs; red dots: Cit-stabilized HAp NPs.

experiments. Figure 2C shows that the thickness of the PAA-stabilized coating is somewhat thicker at lower positive potentials than that by the Cit-stabilized NPs. This can be attributed to the difference in the pK_A of PAA (4.25) and Cit (3.13). This difference implies that it should be easier to protonate PAA than Cit.

EDS element analysis of the coating (Table 2S, Supporting Information, 10×10^{-3} M) revealed relatively large amounts of carbon, indicating that the coating was enriched with Cit. The Cit deposition is attributed to the formation of Ti-Cit complex due to oxidation of titanium to Ti^{+4}.[32,33] Ti-Cit complex is water-soluble and, therefore, large amounts of Ti-Cit in the coating might induce the dissolution of the film and impair the stability of the HAp deposit in aqueous solution. Ti-PAA complex was also reported as water soluble.[34,35] Therefore, different Cit concentrations were examined as shown in Table 2S (Supporting Information). Clearly, as the concentration of the Cit decreased, its content in the coating decreased respectively. Figure 4S (Supporting Information) shows the EDS spectrum and elemental mapping of the coated substrate in low Cit concentration, which definitely confirms that the deposit is composed of pure HAp. We found that the HAp NPs dispersion was not affected, as long as the Cit concentration was higher than 1×10^{-3} M. Therefore, further experiments were conducted with either 1×10^{-3} M Cit or 0.03% (w/w) PAA.

Lowering the concentration of the ionic stabilizer, Cit or PAA, required the addition of an electrolyte to decrease the resistance of the solution. Thus, KNO_3 (10×10^{-3} M) was added. Further inspection of the EDS analyses (Table 2S, Supporting Information) showed good agreement with the expected ratio of Ca/P.[36] The oxygen-to-calcium atomic ratio of stoichiometric HAp is 2.6, therefore only 53% of oxygen is attributed to the HAp while additional 9% of the detected oxygen comes from the Cit molecules. The oxygen-to-carbon ratio in Cit is 2.3, which should give rise to 3.9% of carbon, and therefore, is in accordance with the content that was found (4.1%). Hence, it is evident that most the carbon found in the coating originates from the Cit.

Figure 5SA (Supporting Information) shows the XRD pattern of electrochemically deposited HAp coating on titanium. The four intense peaks are related to the titanium substrate (ICSF-PDF2 file 04-002-2539). Figure 5SB (Supporting Information) shows grazing incidence XRD (GIXRD) with Rietveld refinements, which was performed overnight in order to observe the HAp signal while eliminating the intense peaks of the substrate. These results prove that the coating is composed of HAp.[37] The spectrum of the HAp deposit reveals peak broadening, which is typical to nanocrystalline HAp.[13,38] Indeed, the average crystallite size was between 12 and 18 nm. The hexagonal unit cell parameters were calculated and found to be $a = 9.415$ Å and $c = 6.870$ Å, which is in good agreement with the lattice parameters of stoichiometric HAp ($a = 9.416$ Å and $c = 6.874$ Å, space group $P6_3/m$, based on ICSD-PDF2 file 01-084-1998). Figure 6SA,B (Supporting Information) shows

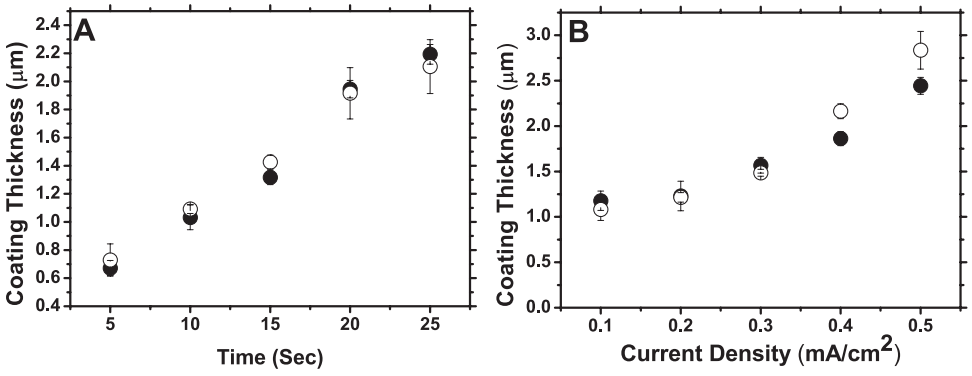

Figure 3. The effect of A) time and B) current density on the thickness of coatings produced by HAp NPs stabilized by either Cit (red symbols) and PAA (black symbols).

the Fourier-transform infrared (FTIR) spectra of the HAp coating stabilized with PAA and Cit. All low bands are attributed to HAp, as shown before.[39,40] Moreover, a broad peak can be seen between 3100 and 3500 cm^{-1} centered at 3260 cm^{-1}. This can be attributed to the stretching vibration mode of OH^- groups.[41] Both are present in HAp, as well as in the PAA and Cit additives. No additional peaks were observed in the spectra.

Figure 3A shows the effect of the duration of deposition on coating thickness upon applying a constant potential of 2 V for 25 min. It can be seen that the thickness of the HAp layer increases linearly, which indicates that the process is Faradaic and that the diffusion layer is not disrupted. This has been previously demonstrated by us in a potential-induced electrochemical deposition of sol–gel.[42,43] Nevertheless, we expect that the process will be self-limiting since the oxidation of water takes place at the Ti/electrolyte interface while deposition occurs at the HAp layer/electrolyte interface. Obviously, the distance between these two interfaces depends directly on the film thickness, which increases over time.

To assure a constant rate of deposition, it is preferable to perform the electrochemical deposition under constant current, as shown in Figure 3B. Specifically, a constant current that varied between 0.1 and 0.5 mA cm^{-2} was applied for 10 min. It is important to note that the current density during the potentiostatic deposition was ≈0.15 mA cm^{-2}. It is evident that increasing the current density slightly increases the deposition rate for current densities below 0.4 mA cm^{-2}. At higher current densities, the rate of deposition increases more significantly; however, the Ti substrate was severely oxidized and the deposition was inhomogeneous.

The tensile stress to failure of the PAA-stabilized coating, as a standard measure of the adhesion of the coating to the substrate, was examined. The samples were first grid-blasted by alumina powder in order to increase the contact area between the glue and the samples, thus ensuring that the failure will not occur between the control sample and the glue. The stress to failure was 17.9 ± 1.5 MPa. ESEM-EDS analysis was used to determine the locus of failure; both parts of the specimen were analyzed. In EDS analysis, Ca and P indicated the presence of HAp on the surface while Si and C were considered as indicators for the presence of glue on the surface. Ca and P were found on both the uncoated glued sample and the coated sample. Glue was found on both sides as well. These findings indicate that the failure was cohesive—either within the glue or within the coating. Hence, the adhesion of the coating to the substrate remained intact, and is expected to be higher than the value shown here. This result satisfies the requirement of the US FDA as well as of ASTM and ISO standards for an adhesion strength of at least 15 MPa.[44]

2.3. Implant Characterization and In Vitro Bioactivity Test

To prove the applicability of our approach toward coating of medical devices, a commercial dental implant made of Ti–6Al–4V alloy was used. It was coated at 2 V for 25 min, as described above. **Figure 4** shows the SEM images of the coated implant. Clearly, the nanoparticulate coating covers well the surface of the implant; the complex geometry of the implant has no detrimental effect on the formation of the coating. Electroplating is very powerful for coating complex geometries, porous structures and non-line-of-sight surfaces. This benefit applies also to the HAp NP electroplating shown here. Since electron transfer is limited to a few nm from the electrode, the formation of a pH gradient will also follow the intimate structure of the surface. Hence, our method is highly appealing for industrial use.

The bioactivity of the coated implant plays a major role in determining the success or failure of the implantation. Therefore, the tendency of the coated implant to promote bone formation was tested by soaking the implant in a simulated body fluid (SBF) at 37 °C. **Figure 5** shows SEM images of the commercial dental implant coated with HAp NPs after soaking in SBF at 37 °C for 30 d.

It can be clearly observed that the morphology of the HAp NPs coating turned into porous interconnected network of HAp layer. The elemental analysis of the coating by EDS is shown in Table 3S (Supporting Information). Normally, the formation of dense apatite layers on bioactive materials is observed after soaking in SBF for a certain time.[45–47] However, the formation of interlinked apatite has rarely been reported.[45] This porous apatite system can promote osseointegration and osteoconduction properties.[48] Moreover, it is shown that after 30 d of incubation, processes of mineralization, nucleation and precipitation occurred presumably due to the interactions of the HAp NPs with the Ca^{2+} and PO_4^{3-} ions in the SBF solution.[45] Previous studies[49] have shown that bone formation

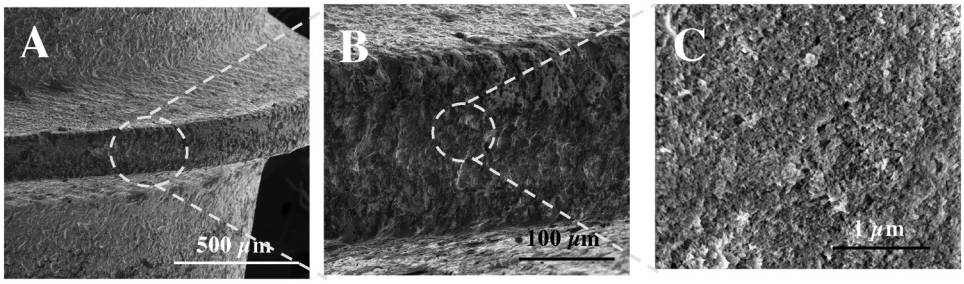

Figure 4. SEM images at different magnifications of a dental implant electrodeposited with HAp NPs stabilized by Cit at 2 V for 25 min.

associated with HAp coating begins with surface dissolution of HAp, which releases Ca^{2+} and PO_4^{3-} into the space around the implant and reprecipitating as new bone. The formation of apatite layer is based on the attraction of ions from the solution by positive (Ca^{2+}) and negative sites (PO_4^{3-} and OH^-) on the HAp. This bioactive nature represents the sign of in vivo formation of bone bonding on the surface of the implant.[47] The bioactivity test also reveals the stability of the electrochemical coating in SBF at 37 °C, which enables the biomineralization of bone-like apatite on a titanium implant. It can be observed that the presence of the organic stabilizer did not interfere with the formation of a new mineralized apatite layer. On the contrary, Cit is one of the bone components and has been reported to be a significant nucleation promoter of apatite crystals.[50,51] Li et al. reported that increased bioactivity of HAp sheets was observed after soaking in citrate-containing SBF compared to regular SBF.[52] It can be assumed that the combination between HAp and Cit as two components of the bone (70 and 0.9 wt%, respectively[51]) can lead to a superior bioactivity of the transplant. Similarly, PAA coating on titanium was reported as both enhancing anticorrosion and promoting osteoblasts function.[34,53]

Elemental analysis (Table 3S, Supporting Information) shows elevated amount of calcium and phosphorus after soaking in SBF, which reflects the bioactivity of the HAp NPs coating. This is related to the enhanced deposition of Ca^{2+} and PO_4^{3-} from the solution. The Ca/P ratio decreases from 1.6 ± 0.1 before soaking to 1.5 ± 0.2 after soaking, but this is not statistically different. The presence of Cl^-, K^+, and Mg^{2+} in the coating also indicates the biomineralization of the HAp coating by absorbing ions from the solution. The loss of carbon in the coating may be related to ion-exchange between Cit/PAA on the NPs surface to phosphate ions in the solution as part of the biomineralization of the implant.

3. Conclusions

For the first time, titanium plates and implants were electrochemically coated by HAp NPs. The proposed electrochemical mechanism involves oxidation of a protic solvent, i.e. water, to generate an acidic environment on the titanium surface. This causes discharge of the negatively charged HAp NPs and their irreversible deposition. Citrate as well as poly(acrylic acid) were used for dispersing the HAp NPs. Both ζ-potential and particle size distribution measurements support this mechanism. HAp coating was obtained both by potentiostatic and galvanostatic deposition in which the thickness of the deposit was very well controlled by the applied potential or current and their duration. Coating of a dental implant with complex geometry was successful, which implies that the process developed herein is well adequate for industrial use. The coated implants were highly bioactive and resulted in the growth of an inorganic film upon soaking in SBF for 30 d at 37 °C. The morphology of the soaked implant confirmed the formation of bone-like apatite layer, which resembles in vitro bone regeneration. This method has proven as highly efficient, straightforward, and economic, hence, could be well implemented in industrial use.

4. Experimental Section

HAp NPs Synthesis: HAp NPs were synthesized using a precipitation method.[10] 4.722 g of $Ca(NO_3)_2$ (ACS EMSURE, Merck, Darmstadt, Germany) was dissolved in 18 mL of high purified water (Barnstead, Dubuque, Iowa, USA) using a magnetic stirrer. The pH of the solution was adjusted to 12 by adding 0.6 mL ammonium hydroxide (25%, Baker Analyzed, J.T Baker, Deventer, The Netherlands) and 17.4 mL water. 1.584 g of $(NH_4)_2HPO_4$ (BioUltra≥99.0%, Sigma-Aldrich, St. Louis, Missouri, USA) was dissolved in 30 mL water while stirring. The pH of the solution was adjusted to 12 by adding 15 mL of concentrated ammonium hydroxide and another 19 mL deionized water. The

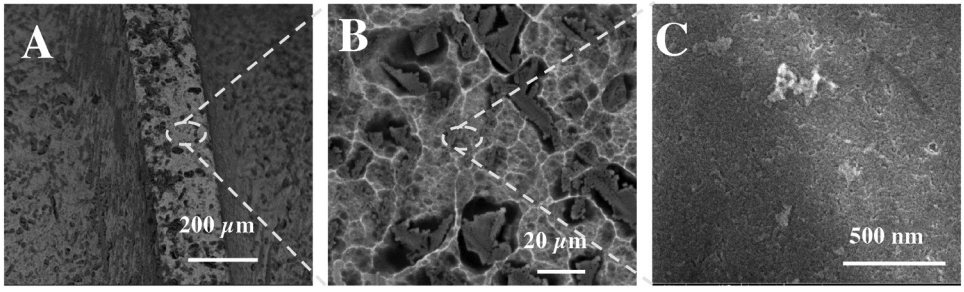

Figure 5. SEM images at different magnifications of a commercial dental implant coated with HAp NPs after 30 d soaking in SBF at 37 °C.

diammonium phosphate solution was slowly added dropwise using a separatory funnel to the calcium nitrate solution while vigorously stirring. The slow addition resulted in a turbid suspension. The latter was boiled for 1 h. Then, the suspension was cooled to room temperature and left until the pH decreased to 7 (after ≈3 d). The precipitated NPs were washed with water and centrifuged at 4000 rpm. This was repeated three times. The so obtained gel-like suspension was collected and freeze-dried using liquid nitrogen. After 48 h, pure HAp powder was obtained. The HAp NPs were characterized by XRD (Bruker, D9 Advance), XPS (Axis Ultra), and extreme high resolution scanning electron microscope (XHR-SEM, FEI Magellan 400L) equipped with energy-dispersive X-ray spectroscopy (EDS). All XRD results were compared to the ICSD (Inorganic Crystal Structure Data) files.

HAp Suspension Preparation: Suspension of HAp was prepared using either tri-sodium citrate (AnalaR, BDH Laboratory Supplies, Poole, England) or sodium PAA ($M_w \approx 5100$ based on gel permeation chromatography, GPC, Aldrich) as dispersing agents. Specifically, 0.5% (w/w) HAp NPs were added to either 10×10^{-3} M citrate (Cit) solution or 0.3% (w/w) PAA solution. Later on, HAp dispersions were prepared at low concentration of Cit or PAA (1×10^{-3} M or 0.03% respectively) with the addition of 10×10^{-3} M KNO_3 (ACS EMSURE, Merck, Darmstadt, Germany). Stable NP dispersions were obtained following sonication of 100 mL solution for 15 min at 100% amplitude, and pulse rate of 1 s on, 1 s off, using tip-sonicator (Sonics, Vibra cell). The suspension stability was examined by measuring the (zeta) ζ-potential and particle distribution size (Zetasizer, Malvern ZS).

Titanium Surface Pretreatment: Ti (Grade 4) plate and Ti–6Al–4V rod were purchased from Bramil LTD. The surface area of the Ti plate was 1.08 cm^2, and that of the Ti–6Al–4V rod was 1.27 cm^2. The Ti plates were manually ground on Grit 600 and Grit 4000 grinding paper (Microcut, Buehler, USA), rinsed in acetone, ethanol, and water in ultrasonic bath (Elmasonic P, Elma) for 10 min, and etched in (40%)HF/(65%)HNO_3 (2 vol% and 20 vol%, respectively) for 1.5 min. Commercial dental implants made of Ti–6Al–4V from SGS Dental Implants (Schaan, Liechtenstein) were tested.

Electrochemical Deposition: Electrochemical deposition was carried out using the potentiostat of a scanning electrochemical microscope (CH Instruments) in a conventional three-electrode cell. Platinum wire (35 mm long) was used as counter electrode, Ag/AgCl [1 M] as reference electrode, pretreated Ti (Grade 4) or Ti–6Al–4V as working electrode. For each experiment, a fresh 17 mL dispersion (0.5% w/w HAp) was used. A constant potential, between 1.5–2.5 V versus Ag/AgCl [1 M] was applied for a given time. During deposition, the solution was moderately stirred. Then, the Ti surface was carefully withdrawn from the solution, washed with clean water, and dried under atmospheric conditions. In another set of experiments, a constant potential of 2 V was applied for different times (5–25 min). Alternatively, a constant current density, between 0.1 and 0.5 mA cm^{-2}, was applied for a certain time. Commercial dental implants were electrochemically coated by applying 2 V for 25 min using PAA (0.03% w/w) as dispersing agent.

Coating Characterization: The coated substrates were analyzed by XRD ($2\theta = 15°–60°$ at step size 0.02° per s) and overnight GIXRD ($2\theta = 24°–35°$ at step size 0.02° per 20 s). High magnification images of the coated surface were taken both by XHR-SEM and by environmental SEM (ESEM, FEI Quanta 200FEG). The thickness of the samples was measured by profiler (KLA Tencor). Element analysis was performed by EDS. FTIR spectra were recorded using Bruker EQUINOX 55 in reflection mode. A liquid-nitrogen-cooled mercury cadmium telluride detector was used for high wavenumbers spectra, while deuterated triglycine sulfate detector was used for low wavenumbers spectra. The samples were scanned 2500 times with 4 cm^{-1} resolution. The spectra were recorded between 400 and 4500 cm^{-1}.

Adhesion Test: The strength of adhesion of PPA-stabilized HAp coating to the metal substrate was tested by a standard tension test. Each test specimen was an assembly of a coated sample and a matching uncoated sample with exactly the same dimensions and surface pretreatment which included grit blasting by alumina powder (high purity white alumina powder from Calbex Mineral Trading, Inc., Henan, China). The blasting machine was model SandyPlus GD from Carlo DeGiordi (Italy). Blasting parameters were: grit size of F200–F180 (59–68 µm), pressure of ≈6 atm, and working distance of 3 cm or higher. The grit blast operation lasted until a dark gray shade evenly covered the sample. The sample was then washed in DI water and cleaned ultrasonically in acetone. The two parts of the assembly were bonded together by a thin layer of a 3M Scotch-Weld Epoxy Adhesive DP–420 Off-White, which was left to cure at room temperature for 24 h while exposing each assembly to a compression stress of 138 kPa (20 psi). The sample was held by grips of an MTS 20/M tensile machine. The tensile load was applied at a constant cross-head velocity of 0.5 mm min^{-1}. This velocity, which is slightly lower than that recommended in ref. [54], was found most suitable for the samples used in this study, where both the cross section and the thickness of the coating were smaller than the values referred to in ref. [54]. Four assemblies were tensile tested. In addition to monitoring the maximum applied load, the locus of failure was determined by inspecting both parts of the assembly by means of ESEM-EDS.

Bioactivity Test: SBF was prepared according to a procedure that was elaborated elsewhere.[45,46] The coated implant was soaked in SBF solution at 37 °C for 30 d in thermostatic bath (Firstek B300). The morphology of the implant was examined by ESEM and XGR-SEM-EDS.

Supporting Information

Supporting Information is available from the Wiley Online Library or from the author.

Acknowledgments

This study was financially supported by a Kamin grant 52694–5 from the Israel Ministry of Economy. The partial support by the Focal Technology Area through the Israel National Nanotechnology Initiative (INNI) is acknowledged. The Harvey M. Krueger Family Centre for Nanoscience and Nanotechnology of the Hebrew University is acknowledged. The authors thank SGS Dental for providing us commercial dental implants to test our coatings. Note added in proof: The work described here is the subject of the following patent: D. Mandler, N. Eliaz, O. Geuli, N. Metoki, *US Patent Application 62/380,810*, filed August 29, 2016.

Received: July 15, 2016
Revised: August 16, 2016
Published online: September 20, 2016

[1] T. Sridhar, N. Eliaz, U. K. Mudali, B. Raj, *Corros. Rev.* **2002**, *20*, 255.
[2] N. Eliaz, T. Sridhar, U. Kamachi Mudali, B. Raj, *Surf. Eng.* **2005**, *21*, 238.
[3] S. R. Paital, N. B. Dahotre, *Mater. Sci. Eng., R* **2009**, *66*, 1.
[4] X. Y. Liu, P. K. Chu, C. X. Ding, *Mater. Sci. Eng., R* **2004**, *47*, 49.
[5] A. Nanci, J. D. Wuest, L. Peru, P. Brunet, V. Sharma, S. Zalzal, M. D. McKee, *J. Biomed. Mater. Res.* **1998**, *40*, 324.
[6] N. Eliaz, M. Eliyahu, *J. Biomed. Mater. Res., Part A* **2007**, *80*, 621.
[7] S.-J. Park, J.-M. Jang, *J. Nanosci. Nanotechnol.* **2011**, *11*, 7167.
[8] H. Wang, N. Eliaz, Z. Xiang, H.-P. Hsu, M. Spector, L. W. Hobbs, *Biomaterials* **2006**, *27*, 4192.
[9] A. Belcarz, G. Ginalska, J. Zalewska, W. Rzeski, A. Slosarczyk, D. Kowalczulk, P. Godlewski, J. Niedzwiadek, *J. Biomed. Mater. Res., Part B* **2009**, *89B*, 102.
[10] M. Wei, A. J. Ruys, B. K. Milthorpe, C. C. Sorrell, *J. Mater. Sci.: Mater. Med.* **2005**, *16*, 319.
[11] N. Eliaz, R. Latanision, *Corros. Rev.* **2011**, *29*, 5.
[12] I. Zhitomirsky, L. GalOr, *J. Mater. Sci.: Mater. Med.* **1997**, *8*, 213.

[13] Z. C. Wang, F. Chen, L. M. Huang, C. J. Lin, *J. Mater. Sci.* **2005**, *40*, 4955.
[14] N. Eliaz, T. M. Sridhar, U. K. Mudali, B. Raj, *Surf. Eng.* **2005**, *21*, 238.
[15] N. Eliaz, W. Kopelovitch, L. Burstein, E. Kobayashi, T. Hanawa, *J. Biomed. Mater. Res., Part A* **2009**, *89*, 270.
[16] Y. Han, S. Li, X. Wang, I. Bauer, M. Yin, *Ultrason. Sonochem.* **2007**, *14*, 286.
[17] M. P. Ferraz, F. J. Monteiro, C. M. Manuel, *J. Appl. Biomater. Biomech.* **2004**, *2*, 74.
[18] M. Šupová, *J. Mater. Sci.: Mater. Med.* **2009**, *20*, 1201.
[19] M. Sadat-Shojai, *J. Iran. Chem. Soc.* **2009**, *6*, 386.
[20] D. G. Shchukin, G. B. Sukhorukov, *Adv. Mater.* **2004**, *16*, 671.
[21] D. Thiemig, A. Cantaragiu, S. Schachschal, A. Bund, A. Pich, G. Carac, C. Gheorghies, *Surf. Coat. Technol.* **2009**, *203*, 1488.
[22] X. Pang, I. Zhitomirsky, *Mater. Chem. Phys.* **2005**, *94*, 245.
[23] M. Farrokhi-Rad, T. Shahrabi, *Ceram. Int.* **2013**, *39*, 7007.
[24] M. Farrokhi-Rad, T. Shahrabi, *Ceram. Int.* **2014**, *40*, 3031.
[25] M. J. Bailey, S. Coe, D. M. Grant, G. W. Grime, C. Jeynes, *X-Ray Spectrom.* **2009**, *38*, 343.
[26] A.-R. Ibrahim, X. Li, Y. Zhou, Y. Huang, W. Chen, H. Wang, J. Li, *Int. J. Mol. Sci.* **2015**, *16*, 7960.
[27] E. Landi, A. Tampieri, G. Celotti, S. Sprio, *J. Eur. Ceram. Soc.* **2000**, *20*, 2377.
[28] I. Levy, S. Magdassi, D. Mandler, *Electrochim. Acta* **2010**, *55*, 8590.
[29] A. Stoch, A. Brozek, G. Kmita, J. Stoch, W. Jastrzebski, A. Rakowska, *J. Mol. Struct.* **2001**, *596*, 191.
[30] M. Wisniewska, T. Urban, E. Grzadka, V. I. Zarko, V. M. Gun'ko, *Colloid Polym. Sci.* **2014**, *292*, 699.
[31] A. Ambrosi, M. Pumera, *ACS Catal.* **2016**, *6*, 3985.
[32] J. M. Collins, R. Uppal, C. D. Incarvito, A. M. Valentine, *Inorg. Chem.* **2005**, *44*, 3431.
[33] Y.-F. Deng, Y.-Q. Jiang, Q.-M. Hong, Z.-H. Zhou, *Polyhedron* **2007**, *26*, 1561.
[34] E. De Giglio, D. Cafagna, M. Ricci, L. Sabbatini, S. Cometa, C. Ferretti, M. Mattioli-Belmonte, *J. Bioact. Compat. Polym.* **2010**, *25*, 374.
[35] H. Li, C. P. Tripp, *Langmuir* **2004**, *20*, 10526.
[36] C. Rey, C. Combes, C. Drouet, D. Grossin, *Compr. Biomater.* **2011**, *1*, 187.
[37] R. Drevet, F. Velard, S. Potiron, D. Laurent-Maquin, H. Benhayoune, *J. Mater. Sci.: Mater. Med.* **2011**, *22*, 753.
[38] Y. Han, X. Wang, S. Li, *J. Nanopart. Res.* **2009**, *11*, 1235.
[39] M. Corno, C. Busco, B. Civalleri, P. Ugliengo, *Phys. Chem. Chem. Phys.* **2006**, *8*, 2464.
[40] J. A. Jansen, B. Leon, *Thin calcium phosphate coatings for medical implants*, Springer, New York **2009**.
[41] X. Zhan, M. Gao, Y. Jiang, W. Zhang, W. M. Wong, Q. Yuan, H. Su, X. Kang, X. Dai, W. Zhang, *Nanomed. Nanotechnol.* **2013**, *9*, 305.
[42] R. Shacham, D. Avnir, D. Mandler, *Adv. Mater.* **1999**, *11*, 384.
[43] R. Shacham, D. Mandler, D. Avnir, *Chem. Eur. J.* **2004**, *10*, 1936.
[44] BS ISO 13779-4:2002, *Implants for surgery-Hydroxyapatite-Part 4: determination of coating adhesion strength*, British Standards Institution, London, UK.
[45] P. N. Chavan, M. M. Bahir, R. U. Mene, M. P. Mahabole, R. S. Khairnar, *Mater. Sci. Eng., B* **2010**, *168*, 224.
[46] T. Kokubo, H. Takadama, *Biomaterials* **2006**, *27*, 2907.
[47] G. S. Kumar, R. Govindan, E. K. Girija, *J. Mater. Chem. B* **2014**, *2*, 5052.
[48] E. K. Girija, S. P. Parthiban, R. V. Suganthi, K. Elayaraja, M. I. A. Joshy, R. Vani, P. Kularia, K. Asokan, D. Kanjilal, Y. Yokogawa, S. N. Kalkura, *J. Ceram. Soc. Jpn.* **2008**, *116*, 320.
[49] A. Siddharthan, S. Seshadri, T. S. Kumar, *J. Mater. Sci.: Mater. Med.* **2004**, *15*, 1279.
[50] C. Li, L. Zhao, J. Han, R. Wang, C. Xiong, X. Xie, *J. Colloid Interface Sci.* **2011**, *360*, 341.
[51] R. Murugan, S. Ramakrishna, *Compos. Sci. Technol.* **2005**, *65*, 2385.
[52] B. Li, L. Huang, X. Wang, J. Ma, F. Xie, L. Xia, *Ceram. Int.* **2013**, *39*, 3423.
[53] C. Treves, M. Martinesi, M. Stio, A. Gutiérrez, J. A. Jiménez, M. F. López, *J. Biomed. Mater. Res., Part A* **2010**, *92*, 1623.
[54] A. Standard, *ASTM International*, West Conshohocken, PA **2008**.